Separation Science and Technology
Publication details, including instructions for authors and subscription information:
http://www.informaworld.com/smpp/title~content=t713708471

The Prediction of Flux Decline and Blinding in Cellular Ceramic Microfiltration Membranes

N. M. Jackson[a]; G. A. Davies[a]; D. J. Bell[a]
[a] Department of Chemical Engineering, UMIST, Manchester, England

To cite this Article Jackson, N. M. , Davies, G. A. and Bell, D. J.(1995) 'The Prediction of Flux Decline and Blinding in Cellular Ceramic Microfiltration Membranes', Separation Science and Technology, 30: 7, 1529 — 1553
To link to this Article: DOI: 10.1080/01496399508010361
URL: http://dx.doi.org/10.1080/01496399508010361

SEPARATION SCIENCE AND TECHNOLOGY, 30(7-9), pp. 1529-1553, 1995

THE PREDICTION OF FLUX DECLINE AND BLINDING IN CELLULAR CERAMIC MICROFILTRATION MEMBRANES

N.M. Jackson, G.A. Davies, D.J. Bell

Department of Chemical Engineering
UMIST, Manchester, England

ABSTRACT

Cellular ceramic membranes have a structure which resembles that of foams. This is not surprising, since a polymer foam is frequently used as a precursor in the manufacturing process. Like all membranes, the processing characteristics are determined to a large extent by the interaction of particles in the suspension or mixture to be treated with the pores of the membrane. If the particle dimensions are near to the dimensions of the pores, then some particles will be trapped, thereby increasing the hydraulic resistance of the media. This will result, in constant pressure filtration, in a decrease in permeate flux. It is therefore important to be able to predict the passage and retention of particles through the media. The retention on the surface to form a cake and within the media is important and should be differentiated, particularly if cleaning by backflushing is to be considered.

In order to investigate particle retention, a definition of the pore structure of the membrane is necessary. In the majority of studies in this field, because of the complexity of the material, a simplified model is used to describe the internal pores of membranes. The pores are assumed to be cylindrical, parallel (and therefore nonconnecting) capillaries. This is quite inappropriate for the membranes considered in this paper. The pores are formed from a highly connected network of shapes with varying size and cross section. In this work, a model to simulate the foam structure is briefly presented and then used to investigate conditions for microfiltration of near-pore-sized particles.

INTRODUCTION

Cellular ceramic membranes are used in many industries to remove particles from fluids. The ability of the material to withstand high temperatures makes these membranes particularly suitable to treat hot gases and molten fluids. As in all applications of membranes or filters, a major consideration is the productivity of the device in practice. A major problem in this regard is the reduction in permeate flux experienced in operation. This is primarily due to the percolation and retention of particles in the membrane media. The result is a reduction in the service time of the filter, and if backflushing or chemical cleaning of a filter is not possible, a reduction in filter life. In both cases, blinding of a membrane increases the operating costs of the process. In the case of ceramic filters, the problem first posed to us which emphasized the need to be able to predict flux decline was an application for filtering molten aluminium to remove slag before casting metal. The process involved batch filtering of the melt. The filter must be able to handle the full batch without blinding since it was not possible to change the filter under processing conditions.

In order to model microfiltration (MF) processes, a description of the pore structure of the membrane is a key requirement. The basic process involves an interaction between particles in the suspension with pores in the medium. There are essentially two limiting cases, if we define at least to start the particle dimensions by a mean diameter, $\bar{D}_p$, and the pore dimensions by a mean aperture diameter, $\bar{d}_a$,

1. If $\bar{D}_p >> \bar{d}_a$, then the particles will not enter the membrane media but will be separated on the surface to form a cake. Under these conditions, as is well known, the filtration characteristics are determined by the structure of the cake. Blinding of the media is not usually important under these conditions, and backflushing can be used to restore the membrane performance.
2. If $\bar{D}_p << \bar{d}_a$, then any filtration is carried out within the membrane. Particles are separated by adhering to the internal surfaces. The theory developed for

depth filtration can be applied successfully to describe the operation. Backflushing and chemical cleaning to remove *particulates* are usually successful for these conditions. Furthermore, the rate of flux decline is relatively slow.

3. The more difficult régime for operation, which for microfiltration and ultrafiltration of particle suspensions is the more common, is when $\bar{D}_p \sim \bar{d}_a$, i.e., near-pore-sized particles. Under these conditions, a cake may be formed, but significant surface and internal fouling of the membrane will take place.

Two basic models have been used in the majority of published work aimed at describing the process of transport of fluids and suspensions of particles in fluids through porous membranes (1). Before considering these, a brief examination of some typical MF membrane structures is perhaps useful. For Figure 1, SEM microphotographs of seven different types of membranes are shown, giving a guide to the pore structure. Figures a and b show a track-etched polymer membrane and a cellular ceramic membrane (Anotec), respectively. In both cases, the pores are nonconnected capillaries extending from the inlet to the outlet faces of the membranes. Figures c and d are examples of fiber membranes: glass (c) and cellulose (d). In both cases, the pores are formed by intersecting or overlapping fibers which form complex pathways of varying shape and cross section. Figure 1e is a stretched polymer membrane, in this case Goretex©, and has, in some ways, a structure similar to 1c (2,3). Figure 1f is an example of a phase-inversion cellulose acetate membrane; this has a foam structure and is unlike any of the previous examples. Figure 1g is a sintered ceramic membrane; the pores in this case are formed as the space between sintered (nearly spherical) particles.

The models to describe transport through membranes are based on one of two basic assumptions:

1. The pores are assumed to be nonconnecting cylindrical capillaries, and for laminar flow, the flux is then defined by the Hagen-Poisseuille equation,

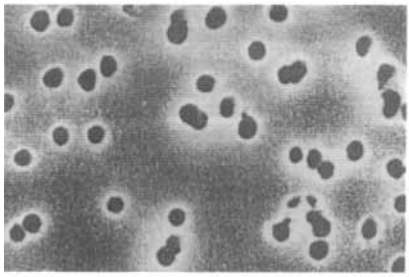

FIGURE 1a.

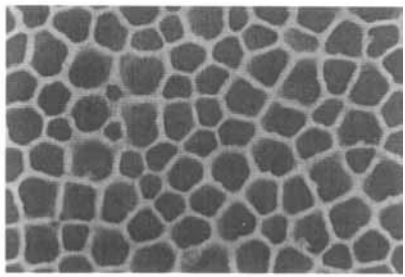

FIGURE 1b.

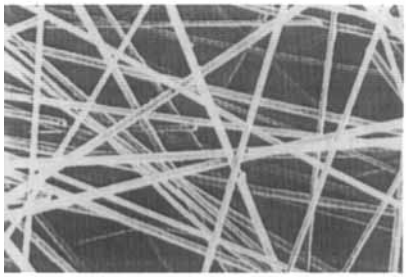

FIGURE 1c.

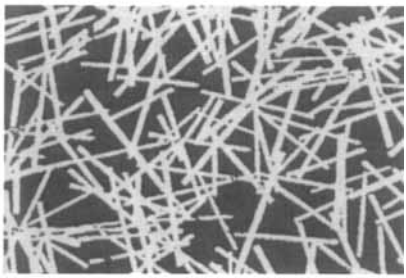

FIGURE 1d.

$$J = \frac{\epsilon_A d^2}{32\mu\tau} \frac{\Delta P}{\Delta Z} \quad (1)$$

where ε_A is the surface porosity or free area of the surface, d is the mean pore (capillary) diameter, μ is the fluid viscosity, and $\Delta P/\Delta z$ is the pressure gradient over the membrane thickness z. A tortuosity factor, τ, is introduced to account for the fact that the capillaries may not be perpendicular to the membrane surfaces. Of the membrane structures shown in Figure 1, only types a and b could be represented by this model, and then only for symmetric structures.

2. The pores are formed by spaces between assemblies of close-packed spheres. The Kozeny-Carman equation is then applied:

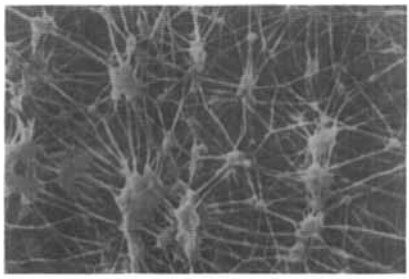

FIGURE 1e.

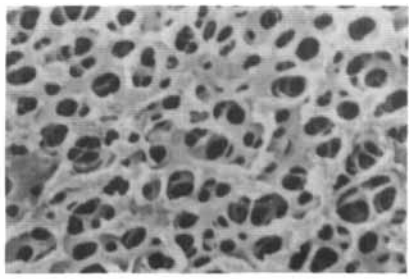

FIGURE 1f.

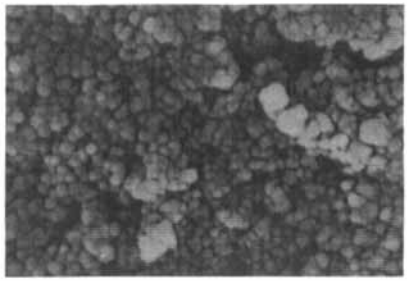

FIGURE 1g.

$$J = \frac{\epsilon_V^3}{K\mu S^2(1-\epsilon_V)^2} \frac{\Delta P}{\Delta Z}. \quad (2)$$

Here, ε_V is the free volume of the membrane, S the internal surface area, and K a constant. This model is only applicable to membranes of the type shown in Figure 1g.

Despite the limited applicability of Equations 1 and 2, they have been applied to interpret data of the range of structures shown in Figure 1. In order to apply these equations, data are required for d, τ, S, ε_A, ε_V, etc. These are frequently obtained from water or air permeability measurements or from mercury intrusion measurements. The interpretation of these measurements requires a description of

the pore structure, and the same equations are used! There can, therefore, be little or no physical meaning in these parameters, and the resulting flux equations must be viewed as no more than an empirical fit of data. Neither approaches, Equations 1 or 2 can be safely applied to cellular ceramic membranes which resemble that in Figure 1g.

Model for the Structure of Cellular Ceramic Membranes

An SEM of a section of a membrane is shown in Figure 2. It is a symmetric structure, so that sections in any orthogonal plane would be similar. The structure resembles a foam or sponge. It is important to recognize that there is no single linear dimension which can adequately define the pores in the membrane. Equations 1 or 2 are quite inadequate to describe the flow through the structure. The pores resemble convex polyhedra. Since the material is usually formed from a polymeric foam precursor, the nodal points in the lattice are not well defined as in nested polyhedra. This is the result of capillary forces which are dominant as the polymer melt or slurry forms the solid phase. The influence of capillary forces forms curved surfaces at the nodal or dislocation points in the lattice. The polyhedral structure persists throughout the media; there are no regions in which the volume elements are isolated, that is, large volumes of solid phase or similarly isolated (nonconnected) void space. In mathematical terms, the volume space is filled with a space exhaustive tessellation. If the centers or nuclei of the individual cells of the tessellation are randomly distributed in 3-dimensional (a Poisson distribution) then the tessellation is a Voronoi tessellation (4). This produces a set of polyhedra which are produced from the nuclei points if a constant isotropic growth process is considered. This would produce a set of spheres which are allowed to expand beyond the position of contact with neighbouring spheres. The growth will then take place along the planes of contact until the space is fully divided. A set of polyhedral cells will then be produced. This is the principal conjecture of a statistical model to describe the porous structure shown in Figure 2 (5). If the number density of cells in the real structure is N, then this defines the

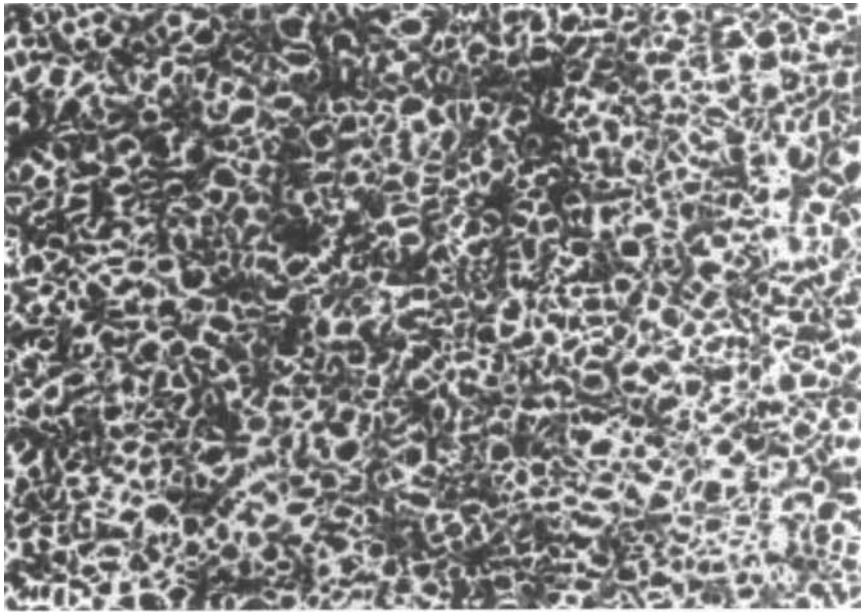

FIGURE 2. SEM photograph of a membrane section.

number of Poisson points. The pores in the membrane will now be defined as the individual cells formed by the interconnecting ceramic filaments. Thus, in the Voronoi tessellation, a pore is equivalent to a Voronoi polyhedron. The Voronoi region of pore i is π_i and is defined by:

$$\pi_i = \{x | d(x,x_i) < d(x,x_j) \quad for\ all\ j \neq i\}, \tag{3}$$

where $\mathbf{x}_1, \mathbf{x}_2,...,\mathbf{x}_i,...,\mathbf{x}_N$ are the coordinates of nuclei in the unit volume V, and d($\mathbf{x}$, $\mathbf{y}$) is the Euclidean distance between $\mathbf{x}$ and $\mathbf{y}$. In other words, π_i is the set of points that is nearer to the nucleus $\mathbf{x}_i$ than other $\mathbf{x}_j$'s.

A structure produced from this definition will take the form shown in Figure 3. At first sight, this may resemble a gas-liquid foam but does not as yet represent a membrane structure of the type considered here. The edges defining polyhedra,

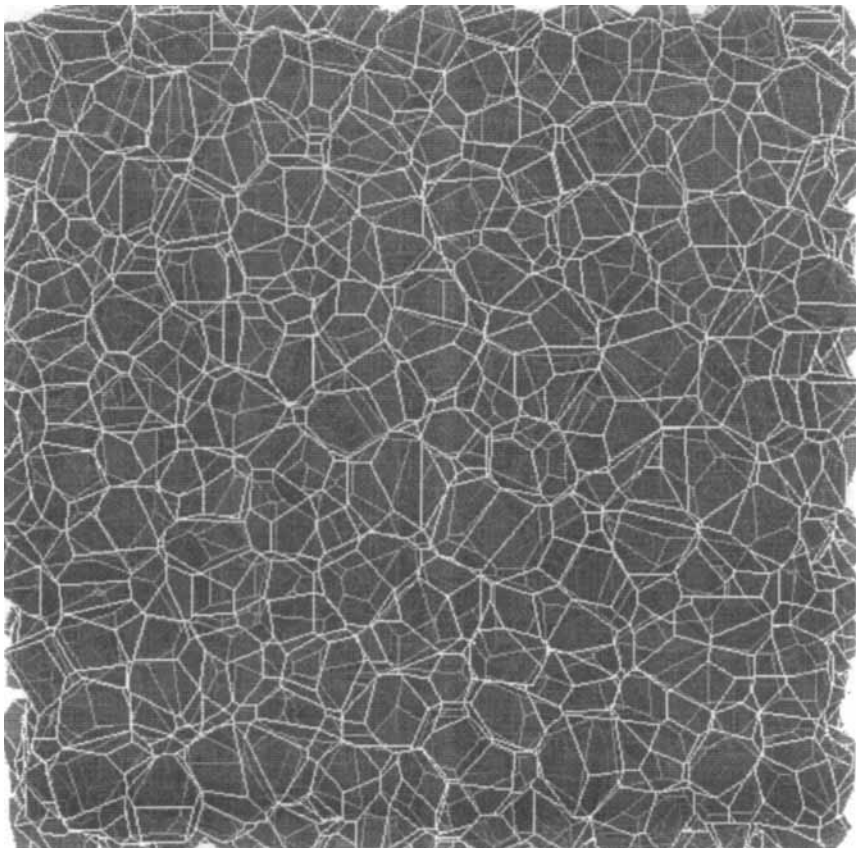

FIGURE 3. A 3-dimensional Voronoi tessellation.

which in the real structure are filaments of ceramic material of finite thickness,are represented as thin lines. The structure in Figure 3 would have a free volume, ε_V, approaching unity, whereas in ceramic membranes, ε_V~0.5-0.6. In addition to this problem, an analysis of the polyhedral volume distribution in a Voronoi tessellation reveals that the distribution is somewhat wider than in actual foams. This can be addressed by imposing a constraint condition on the N Poisson points first defined. A condition can be introduced to accept only those points with a

minimum distance from all other local points. The finite edge thickness of pores can be simply introduced by assuming that these edges are cylindrical rods of constant diameter. The diameter between rods may vary, but for each individual edge, it is assumed constant. This is a simplification which could be refined, since measurements of Plateau (6) borders in foams show again that the influence of capillary forces produce films whose thickness increases toward the nodal points. The computation of this is possible, but the effect is considered of second order and at this stage does not warrant the great increase in computation which would be involved. If ε_V is known for an actual membrane, and if the mean edge thickness, diameter d_e, is estimated, then a simulation of a membrane according to this model can be produced. In Figure 4, an SEM of a surface of a ceramic membrane, 4a, is compared to that produced from the model, 4b. A 3-dimensional image of the model structure is shown in Figure 5. Here, the free volume is deliberately increased to show the internal structure of the membrane and the cellular shapes of the pores. Before proceeding further, it is important to compare the predictions of the model in relation to structural measurements and to compute data from the model for subsequent use in predicting performance. Measurements of structure can be made from SEM microphotographs. At this stage, these are only available of planar sections. It is not yet possible for us to obtain fracture sections along edges of individual pores and thus explore the edge sections. The planar sections were submitted to image analysis using a digitizer. The post areas of the section shown in Figure 4a as dark regions were measured and a cumulative distribution computed. The areas were normalized to the measured mean value. The computations from the model structure are compared with measurements in Figure 6. The computations were made on a Voronoi tessellation of 2158 points (polyhedra). A good agreement between the measurements and the model is shown. A second comparison is the measured pore perimeter, again on a normalized basis. These results are shown in Figure 7. In this case, the fit is slightly less satisfactory. One difference is due to the omission of capillary effects at nodal points which increases the errors for large pores with many edges to a

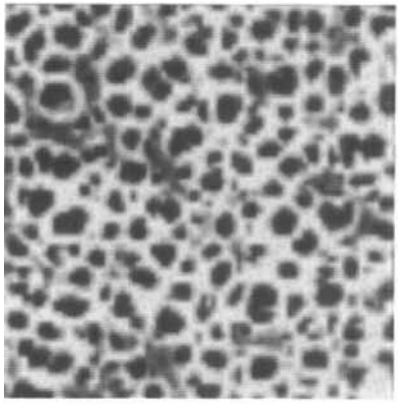

FIGURE 4a. SEM of membrane surface.

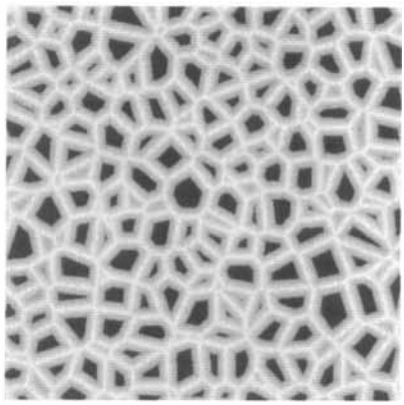

FIGURE 4b. Model of membrane surface.

face. Nevertheless, the model provides a quantitative structure comparable to the membrane structure and can produce data on statistical variations of measurements of facial properties that compare to actual data. Previous attempts based on either deterministic models or assumed structures are incapable of providing even the most fundamental statements on these properties.

The tessellations proposed can be used to provide data on a full range of properties that describe the cellular structure (7). The expected pore volume, $E(V_p)$, is of course dependant only on ε_V and N, thus:

$$E(V_p) = \frac{V\varepsilon_V}{N}. \tag{4}$$

However, the pore volume frequency, $f(V_p)$, can be determined. For each pore, the following expected values, and distribution functions, defined by E and f respectively, can be computed: faces per polyhedron, n_f; the edges per polyhedron face, n_{fe}; the area per polyhedron face, a_f (Figure 6); the perimeter per face, p_f (Figure 7); and the perimeter per polyhedron, p. In considering particle percolation through the lattice, a_f will be important; p_f and p will be important in

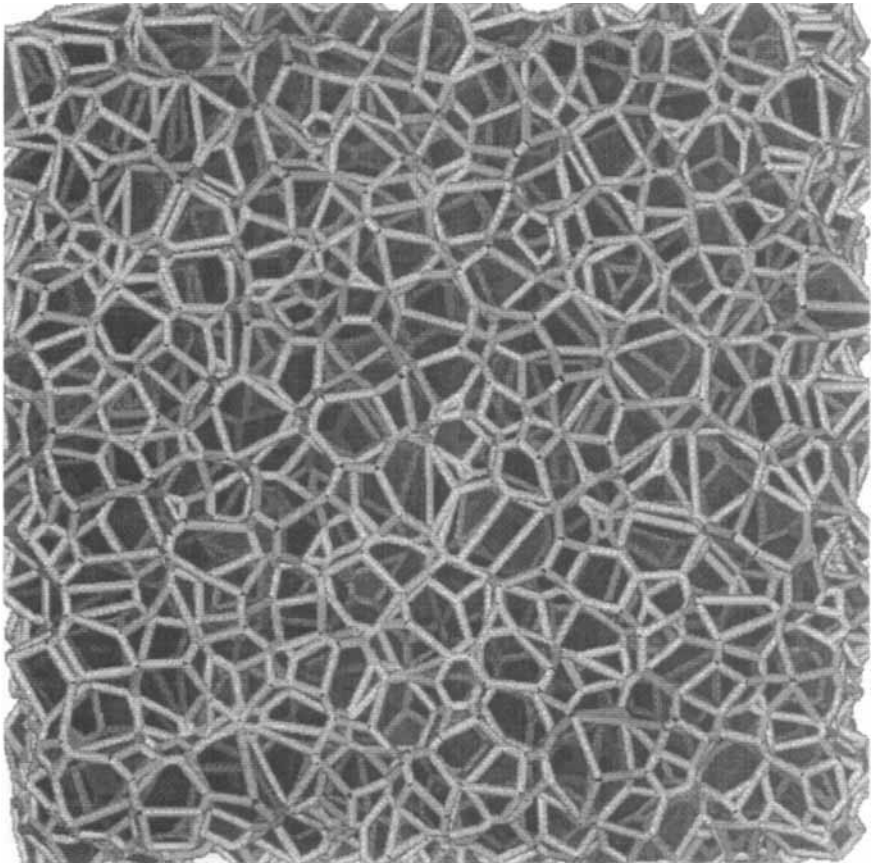

Figure 5. A 3-dimensional structural model with finite edge thickness.

determining the pressure drop for clean solvent flow. Examples of some of the data produced are shown in Figure 8.

Prediction of Particle Transport Through the Membrane

We are interested here in the more difficult case of the filtration of near-pore-sized particles. These will either

1. enter the membrane and pass through in the permeate or be retained to blind the internal structure (fouling);

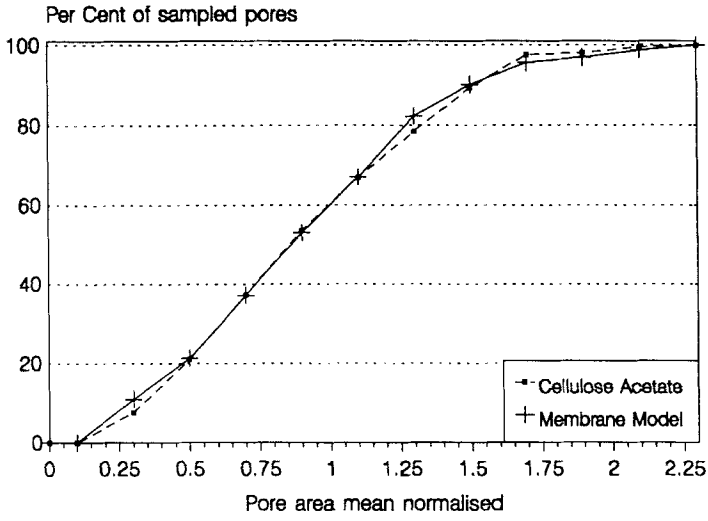

FIGURE 6. A comparison between membrane and model pore areas.

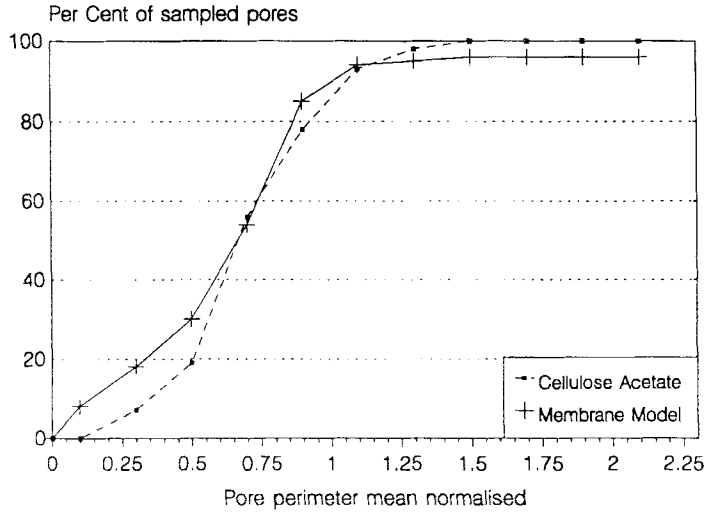

FIGURE 7. A comparison between membrane and model pore perimeters.

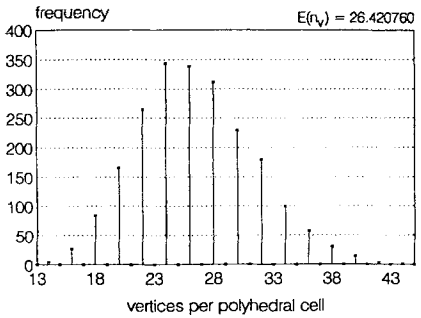

FIGURE 8a. Vertices (nodes) per polyhedron.

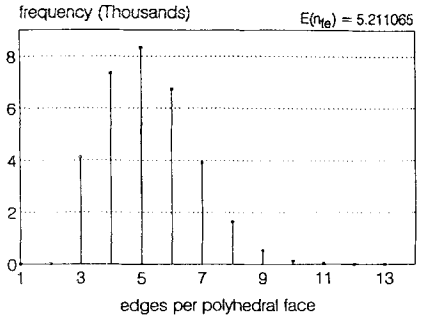

FIGURE 8b. Edges per polyhedron face.

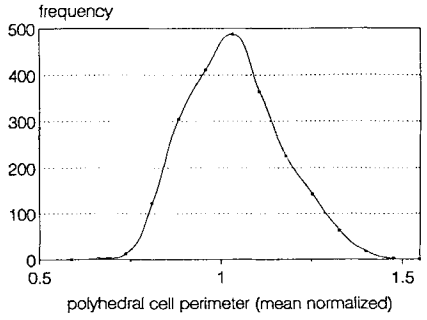

FIGURE 8c. Perimeter per polyhedron.

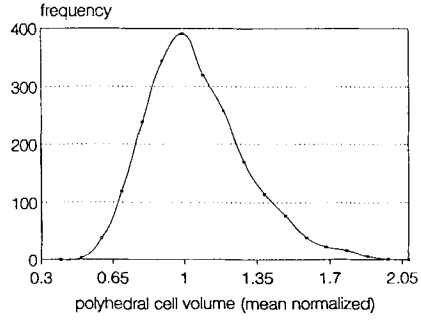

FIGURE 8d. Volume per polyhedron.

2. be retained on the surface and blind the surface pores by becoming 'wedged' (a surface layer will then form); or
3. if filtration beyond the point of surface blinding is continued, a cake will be formed which will ultimately become the filtration media.

These conditions, when $D_p \sim d_a$, are determined mainly by steric effects. We will consider the process of filtration of suspensions of spheres. This can be handled in a computational algorithm based on the model structure proposed and can be validated using suspensions of classified data particles.

A stochastic trajectory model is used to compute the penetration of pore-sized particles with the membrane lattice. The model is based on the computation of independent random walks to describe the particle pathways. First, the suspension process in 'dead-end' filtration, is assumed to be statistically homogenous and described by a concentration, C_o; mean particle diameter, $\bar{D}_p$; and standard

$$D_{pi} = \overline{D_p} + \sigma_p \left[\frac{\sum_{k=1}^{M} x_k - \frac{M}{2}}{\sqrt{M/12}} \right], \tag{5}$$

deviation, σ_p. A particle is chosen from this distribution at random D_i and a random position of entry of this particle into the membrane (x_i,y_i) (measured on the inlet surface) initially at $z_i = 0$. The random walk of this particle is then computed within the pore network. Thus, setting i=1, D_{p1} is determined from the central limit theorem (Equation 5) where x_K is a uniformly distributed random variable $0 \le x_K \le 1$, and M is an integer $M \ge 12$. The position $(x_1,y_1,z = 0)$ of particle 1 is defined again using uniformly distributed random variables such that $0 \le x_1 \le 1$ and $0 \le y_1 \le 1$. The coordinates of the inlet surface of the membrane are normalized such that the x and y axes are between 0 and 1; the thickness z is also normalized between 0 and 1. Having set x_1, y_1 and D_{p1}, and assuming steady laminar plane flow of fluid through the membrane, the face of the nearest Voronoi cell on the surface to x_1 and y_1 is determined. The diameter of the largest inscribed circle, d_a, of this face is then compared to D_{p1}. If $D_{p1} > d_v(x_1,y_1,0)$, then the particle will only partially enter the pore blocking it for further processing. If $D_{p1} < d_a(x_1,y_1,0)$ and $D_{p1} < d_v(x_1,y_1,0)$, then the particle enters the pore. It is assumed that the particles will percolate through the lattice in the pressure gradient. Therefore, the faces in this pore downstream of the inlet face are interrogated to determine if $D_{p1} < d_a$. If more than one face satisfies this condition, then the particle is allowed to pass into the adjacent pore which shares the largest face area (largest inscribed circle diameter). If $D_{p1} < d_a$ for all the faces other than the inlet, then the particle remains in this pore. If for downstream faces $d_a \le D_{p1} \le 1.1 d_a$, then the particle is assumed to

blind the pore face (irreversible by backflushing). If the particle passes to an adjacent pore, the process is repeated. The random pathway followed is computed until either a pore condition is attained where $D_{pi}>d_v$ or $D_{pi}>d_a$, whereupon the trajectory is terminated and the particle is retained in the pore structure. The position (x_i,y_i,z_i) of the particle is then recorded with the particle diameter, D_{pi}, and total path length traversed, l_i. If $z_i = 1$ and the outlined conditions for capture have not been attained, then the particle is assumed to have passed through the membrane with the permeate fluid. The process is then repeated for a second particle, D_{p2}, following exactly the same procedure. As the number of particles processed increases, two additional factors have to be considered:

1. A particle cannot enter a pore that is already occupied by another particle. Then, unless it can escape by penetrating a neighboring pore, it will remain effectively building up a particle cluster within the membrane.
2. If the face of the pore at the surface is already occupied, then an arriving particle cannot enter the membrane at this point even if the local condition, $D_{pi}<d_a(x_i,y_i,0)$, at this point would permit this. Instead, the particle is assumed to roll away from the captured particle, and pores adjacent to this point are examined. If all local pores are occupied, then the particle is assumed to rest in a stable condition on top of the captured particles at this point on the surface. The particle is allowed to roll and come to rest when it contacts at least three particles, thus forming a cake. As the surface becomes covered with particles, a cake forms rapidly.

The qualitative results of the computation procedure are shown in the graphics in Figures 9 and 10. In Figure 9, a section in the x/z or y/z plane is shown. The capture of particles within the structure is seen, as well as the formation of a surface layer and a cake. The development of the cake increases as the process continues. It is evident from the figure that the deposit within the membrane decreases rapidly from the inlet, as is expected from experimental work (8). In Figure 10, a view of the surface plane is shown, which illustrates the development of the surface layer and the cake.

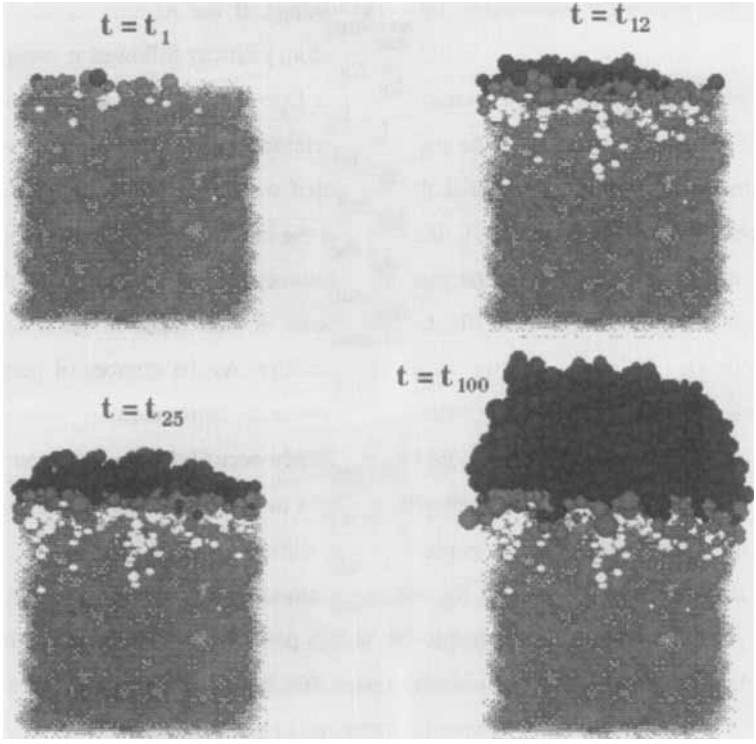

FIGURE 9. Surface cake formation and particle penetration through the model.

The cake forms first as small 'islands' of particles forming local bridging over the surface layers. As the filtration proceeds, these islands coalesce to produce a complete cake. The mechanism of capture of particles within the pores is shown graphically in Figure 11. This shows two fouled pores, the particle on the right blocking a pore and the left-hand particle blinding a second pore. From the calculations, quantitative results can be produced.

Quantitative Predictions for Dead-End Filtration of Suspensions of Latex Spheres

In terms of filter life and performance, the penetration of particles into the filter is important. This constitutes fouling which will reduce the life span of the

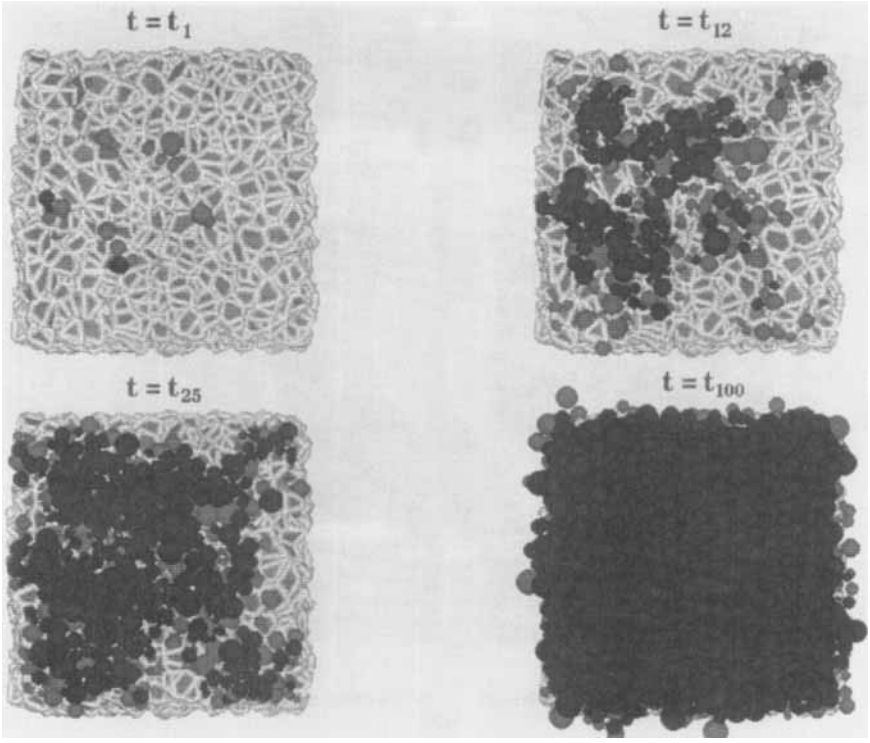

FIGURE 10. Cake formation on the membrane model surface.

membrane and increase the processing time. The results have been computed showing the deposit of particles in the filter as a function of the position from the inlet, z. The effects of the particle size distribution or deposition have been investigated, $\bar{D}_p$ and σ_p. These are reported as dimensionless quantities α and β where $\alpha = \bar{D}_p/\bar{d}_a$ and $\beta = \sigma/\bar{D}_p$. The results, when presented in this form, should be applicable to a wide range of filter types and ratings, $\bar{d}_a$, providing the internal pore structure is described by the structural model developed here. Considering first particle penetration, the results computed in terms of the volume of the solid particles captured in the filter, V, are shown in Figures 12a and 12b. The results

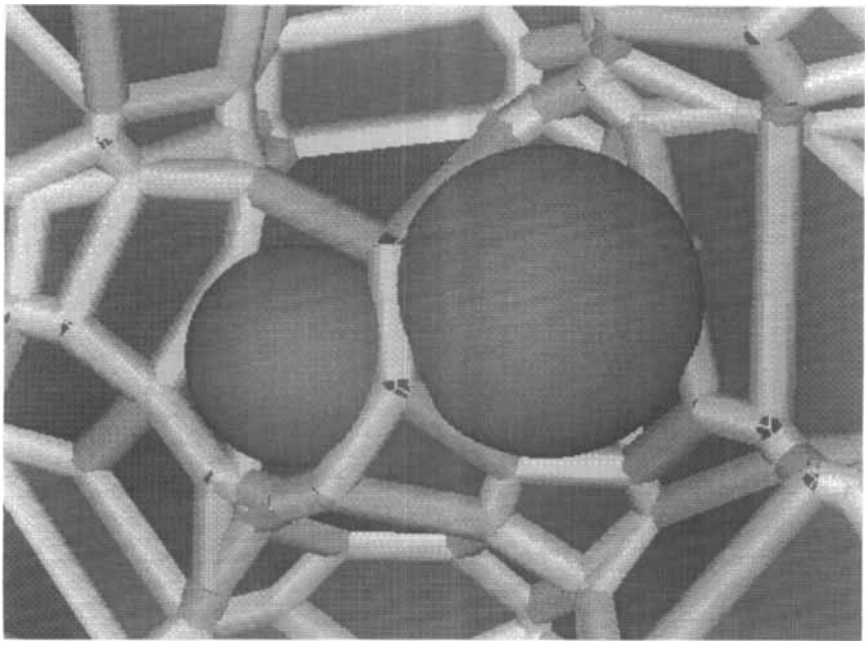

FIGURE 11. Example of pore blocking and blinding.

in 12a at $\beta = 0$ represent the limiting case of filtration of a monodispersion. It is seen that first the penetration into the membrane falls rapidly with distance from the inlet surface. Furthermore, the penetration decreases as α increases, and as $\alpha>1$, retention in the surface layer also decreases. Both results are expected and agree with experimental results. At $\beta = 1.5$, the fractional volume of particle s entering the membrane decreases at equivalent α values, and the deposition becomes slightly more smeared out, a result of an increase in the number of small particles. As α increases, the deposition takes place on the surface to form a cake and the filtration performance is then dominated by the characteristics of the cake, ε_v. The penetration of particles into the membrane decreases rapidly as a cake forms on the surface - again a result which is observed in practice. The deposition with the membrane under these conditions still depends on β and hence, on the

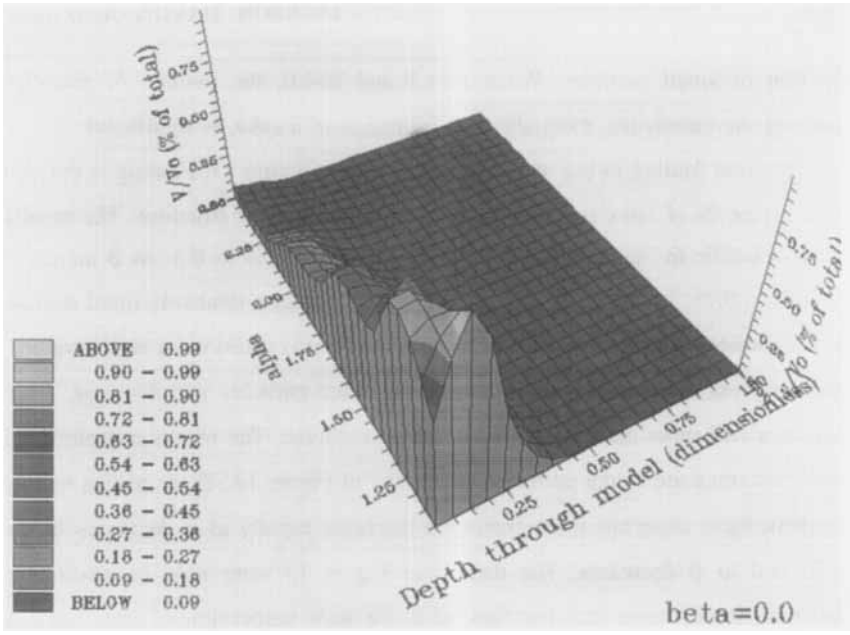

FIGURE 12a. Particle capture, $\beta = 0.0$.

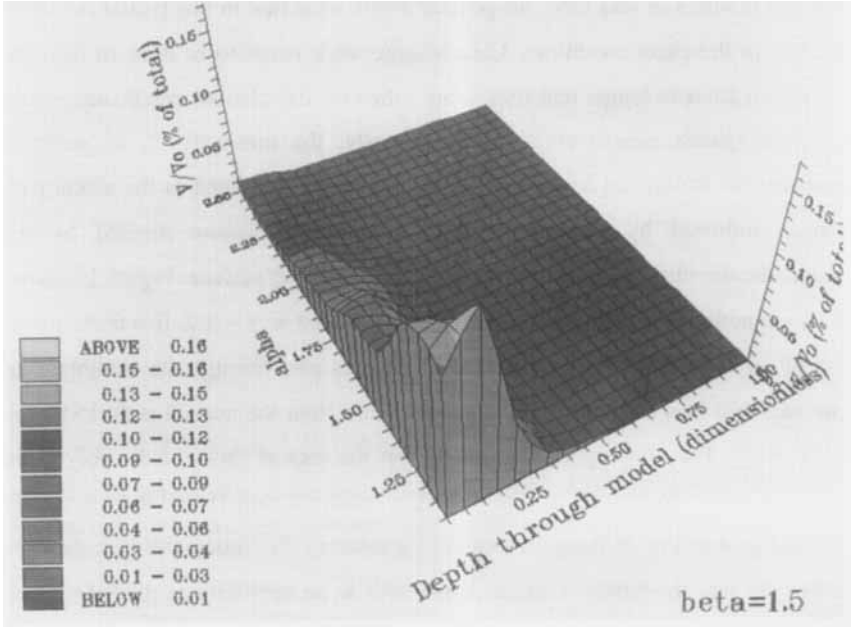

FIGURE 12b. Particle capture, $\beta = 1.5$.

fraction of small particles. When $\alpha \leq 1.5$ and $\beta > 1.0$, the number of particles entering the membrane, even after the formation of a cake, is significant.

Internal fouling in the membrane is shown in Figure 13. Fouling is defined here as the % of latex particles fouling the internal filter structure. The results show a saddle in the surface, extending from $\alpha \approx 0.9$ to 0.5 as β increases from 0 to 0.75. In this range, the model would predict a relatively rapid decline in the permeate flux, particularly when compared with conditions at high α values. Similarly, as α decreases, the number of internal particles will decrease, since particles will more easily pass through the membrane. The results computed for particles entrained in the permeate are shown in Figure 14. These results merely confirm these expectations: entrainment increases rapidly as α decreases below 0.75 and as β decreases. The data from Figure 13 were used to predict the decrease in permeate flux for flow of a 1% wt/v suspension of latex spheres (mean diameter 0.22 μm) in water through a cellular membrane with a pore rating of 0.2 μm. The clean water flux of this system was measured as 0.1 $m^3m^{-2}d^{-1}bar^{-1}$. The decrease in flux predicted is shown in Figure 15. The computation only extends to 400 s of real time, the predicted flux reduction in this period is 6.39% relative to the clean conditions. Clearly more work needs to be done to increase the calculations to longer real-time values; then the calculations can be accurately checked against experimental results. Initially, the tortuosity, τ, of particles entering the membrane has been calculated. Here, τ is defined as the actual path length followed by particles up to the point of capture divided by the perpendicular distance from the capture site to the inlet surface. Figure 16 shows τ as a function of α and β. A maximum is predicted at $\alpha \approx 1.2$, $\beta = 0$. At $\alpha \approx 05$, τ tends to 1, indicating that these small particles pass through the membrane or are captured in a cell with little or no deviation from the normal path. $\tau > 1$ even at $\alpha \approx 2.5$. This may appear surprising, but the area of faces of the polyhedral cells are not uniform (as is evident from the structural model), and there is clearly a finite probability of these large particles entering the lattice and percolating a little way into the lattice. τ can be considered as an approximate guide to assess

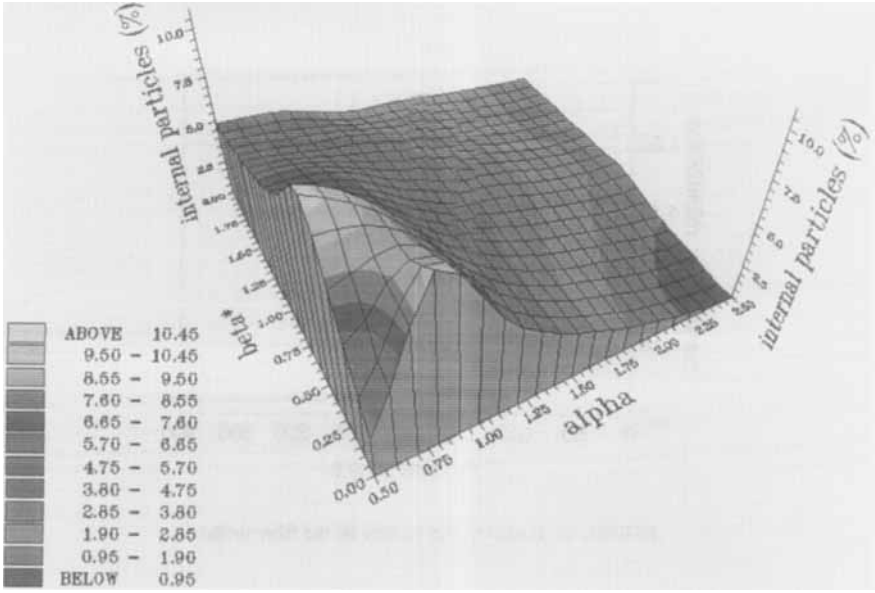

FIGURE 13. Internal fouling of the filter by particles at varying distributions.

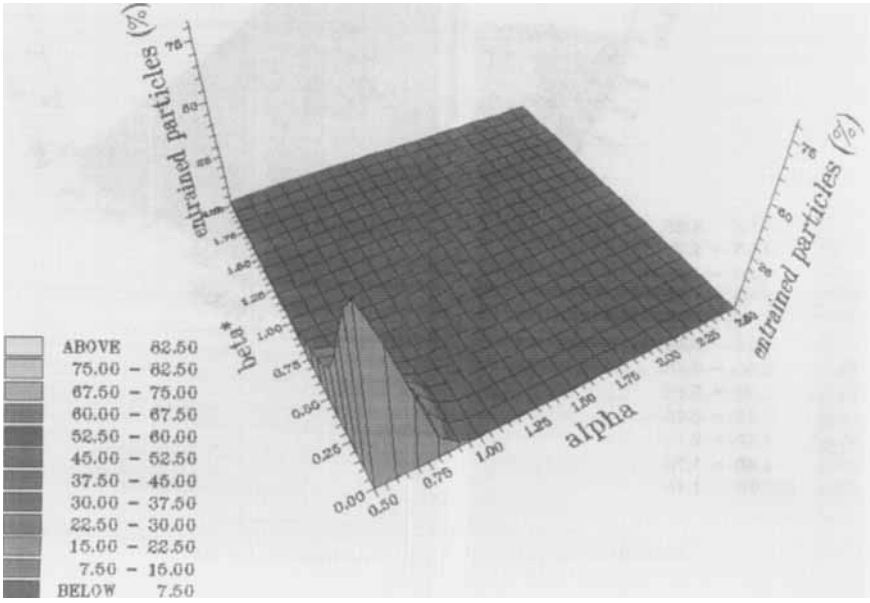

FIGURE 14. Percentage of particles entrained with the permeate.

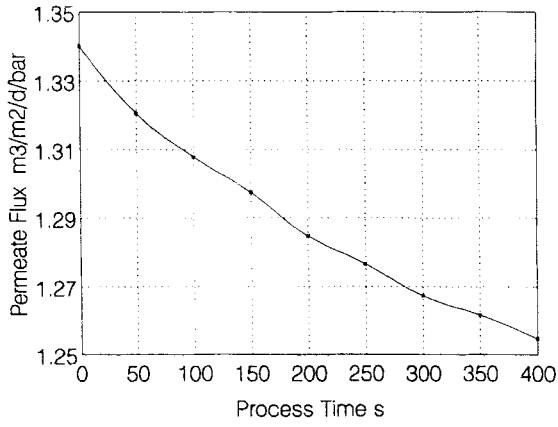

FIGURE 15. Predicted flux decline by the filter model.

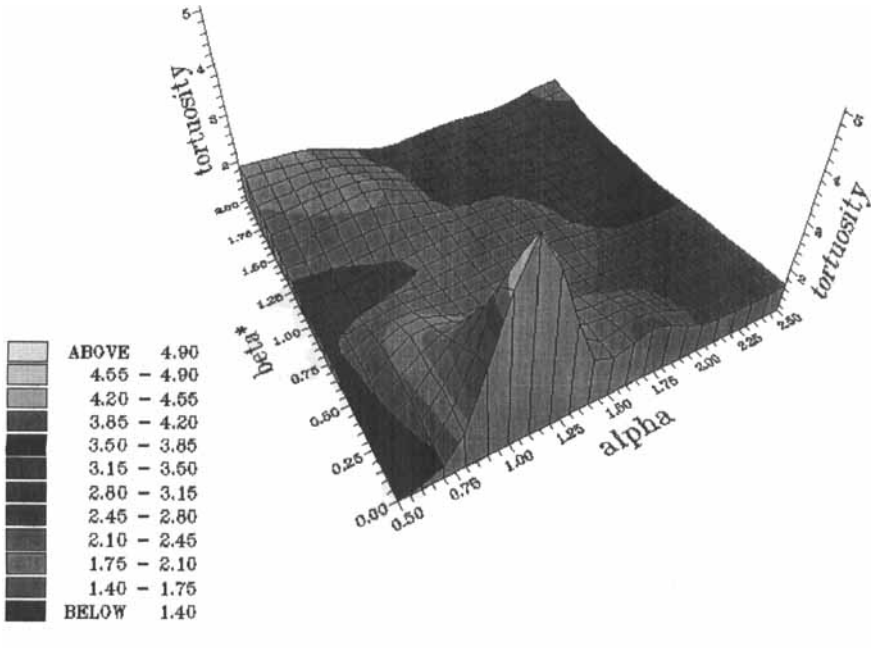

FIGURE 16. Tortuosity of the filter as a function of α and β.

the potential for backflushing. An assumption is made that particles follow independent random walks into the membrane structure and, if the flow is reversed as in backflushing, will describe independent random walks toward the inlet surface. If τ is high, the probability for particle removal will be reduced. Thus, the model suggests that backflushing will be difficult for suspensions in which α is between ~0.9 and 1.3.

CONCLUSIONS

The model proposed to simulate the structure of cellular membranes, based on a 3-dimensional Voronoi tessellation, provides a qualitative description that agrees well with SEM photomicrographs of real membranes. The model assumes that the pores are random convex polyhedra. The quantitative predictions from the model with respect to the pore section area and perimeter at the surface agree well with measurements made from SEM data with a digitized image analyzer. The model is able to provide detailed information on distribution functions of the properties of the polyhedra, many of which relate to the prediction of flux data and fouling.

Using the structural model in conjunction with a description of particle-pore interactions experienced in dead-end filtration, predictions are made on the deposition of particles on the inlet surface and within the structure of the membrane. The latter process is responsible for membrane fouling. Near-pore-sized particles have been studied. Fouling is predicted to be significant if the particle: pore diameter ratios, α, are within the range 0.75-1.25. The fouling is also shown to depend on the dispersion of the particle size distribution, described in terms of the standard deviation. Particle entrainment through the membrane becomes dominant when $\alpha<0.5$. The tortuosity, τ, of particles entering the membrane, is a maximum for α values in the range $0.8<\tau<1.2$. It is likely that if τ is high, backflushing of the membrane to restore the permeate flux to that of the original membrane will be difficult. More work is being carried out to confirm this.

NOMENCLATURE

a_f	area of a face of a polyhedron (pore)	L^2
$\bar{D}_p$	mean particle diameter	L
D_{pi}	diameter of particle i	L
$\bar{d}_a$	mean diameter of the largest inscribed circle of a polyhedron face	L
d_a	diameter of the largest inscribed circle of a polyhedron face	L
d_v	diameter of the largest inscribed sphere of a polyhedron	L
$d(x,x_i)$	distance of nucleus i from a point	L
E( )	expected value of a parameter	-
f( )	distribution of a parameter	-
J	permeate flux	$L^3L^{-2}T^{-1}$
K	permeability coefficient	-
k	summation term	-
l_i	path length of particle	L
M	integer M≥12	-
N	number of polyhedron cells per unit volume	-
n_f	number of faces of a polyhedron	-
n_{fe}	number of edges per face of a polyhedron	-
n_v	number of vertices per polyhedron	-
ΔP	pressure differential	$ML^{-1}T^{-2}$
p_f	perimeter of a polyhedron face	L
p	perimeter of a polyhedron	L
s	process time	T
t	computer time	T
V	volume	L^3
V_p	volume of a pore	L^3

x_i,y_i,z_i	coordinate of particle i	-
x_k	uniformly distributed random variable $0 \leq x_k \leq 1$	-
Δz	depth through membrane	L
α	dimensionless diameter ratio $\bar{D}_p/\bar{d}_a$	-
β	variance ratio $\sigma_p/\bar{D}_p$	-
ε_A	free area of a section of membrane	-
ε_V	free volume of membrane	-
π	Voronoi polyhedron volume	L^3
σ_p	standard deviation of particle deviation	L
μ	fluid viscosity	$ML^{-1}T^{-1}$
τ	tortuosity	-

ACKNOWLEDGMENTS

The authors would like to thank AEA Technology, Biosep for support and encouragement to carry out this work. One of us (NMJ) wishes to thank SERC for the award of a research scholarship.

REFERENCES

1. M. Mulder, Basic Principles of Membrane Technology, Kluwer Academic Publishers (1991).
2. S.T. Arnold and G.A. Davies, J. Mem. Sci. 70, 85 (1992).
3. A.R.N. Fairclough and G.A. Davies, Chem. Eng. Comm. 92, 23 (1990).
4. R.E. Miles, Proc. Nat. Acad. Sci. 52, 901, 1157, (1964).
5. N.M. Jackson, MSc Dissertation, University of Manchester Institute of Science and Technology, U.K. (1991).
6. J.L. Meijering, Phillips Res. Rept. 8, 270 (1953).
7. C. Tien, Granular Filtration of Aerosols and Hydrosols, Butterworth Press (1989).